CHEMISTRY
AN ASIAN JOURNAL
ACES
FOCUS REVIEW

DOI: 10.1002/asia.201300630

Nanoelectronics Meets Biology: From New Nanoscale Devices for Live-Cell Recording to 3D Innervated Tissues

Xiaojie Duan*[a] and Charles M. Lieber*[b]

Dedicated to Professor Chunli Bai on the occasion of his 60th birthday

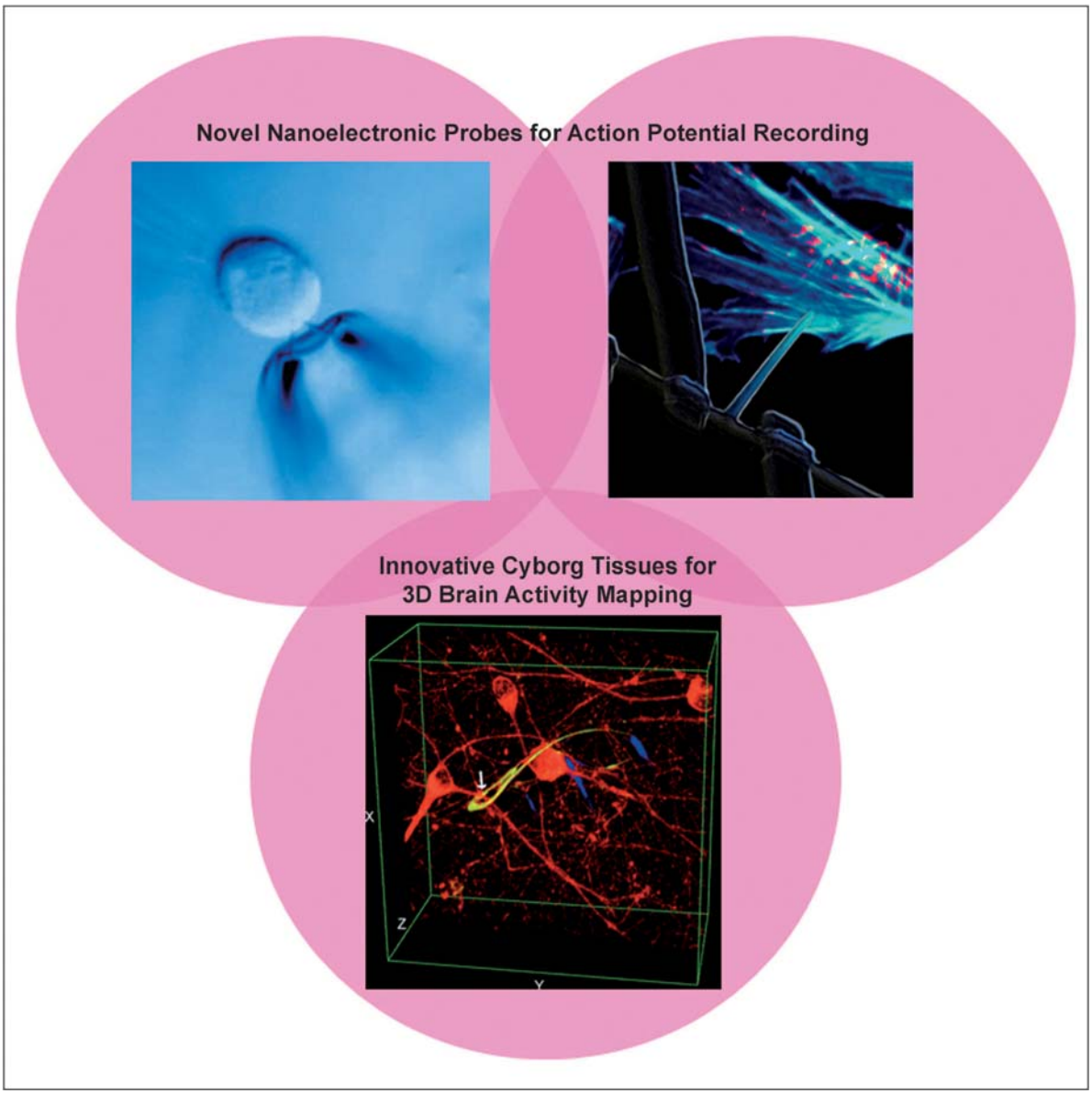

Abstract: High spatiotemporal resolution interfaces between electrical sensors and biological systems, from single live cells to tissues, is crucial for many areas, including fundamental biophysical studies as well as medical monitoring and intervention. Herein, we summarize recent progress in the development and application of novel nanoscale devices for intracellular electrical recording of action potentials and the effort of merging electronic and biological systems seamlessly in three dimensions by using macroporous nanoelectronic scaffolds. The uniqueness of these nanoscale devices for minimally invasive, large-scale, high spatial resolution, and three-dimensional neural activity mapping are highlighted.

Keywords: bioelectronics · electrochemistry · field-effect transistors · flexible electronics · nanostructures · neural mapping · synthetic biology

Introduction

Recording electrical signals from cells and tissues, such as action potentials in the nervous system, is central to areas ranging from fundamental electrophysiological studies to brain activity mapping and biomedical prosthetic applications.[1] Conventional methods based on glass micropipette electrodes have been widely used for intracellular action potential recording and have shown excellent signal-to-noise ratios (SNRs) and temporal resolution. However, these methods have constraints[1b,c,2] that limit their applicability to simultaneous measurements from large numbers of cells with single-cell resolution. In addition, the typical micrometer size of these probes poses a challenge for recording from small subcellular structures and also results in invasiveness and toxicity to cells.[1b,2] On the other hand, methods involving microfabricated metal electrodes and arrays (MEAs) have made large-scale multisite recording possible, although the size of these electrodes remains on the micrometer scale to meet electrode/electrolyte interface impedance conditions necessary to achieve usable SNRs. This size restriction precludes the subcellular resolution needed for many important studies.[1d,e,3] In the case of tissue-level electrical measurements, implementing electronic sensors in three dimensions (3D) and the capabilities for monitoring cells throughout the 3D micro-environment of tissues is critical for functional neural activity mapping and understanding physicochemical changes relevant to living organisms.[1a,4] Most work has, however, focused on coupling electronics to the surface of tissues or artificial tissue constructs, including recently reported studies on flexible and/or stretchable planar devices that conform to tissue surfaces.[5]

[a] Prof. X. Duan
Department of Biomedical Engineering
College of Engineering, Peking University
Beijing 100871 (P.R. China)
E-mail: xjduan@pku.edu.cn
Homepage: http://en.coe.pku.edu.cn/faculty/faculty_143.htm

[b] Prof. C. M. Lieber
Department of Chemistry and Chemical Biology
and School of Engineering & Applied Sciences, Harvard University
Cambridge, Massachusetts, 02138 (USA)
E-mail: cml@cmliris.harvard.edu
Homepage: http://cmliris.harvard.edu/

The nanometer size of nanoelectronic devices makes them advantageous for realizing high resolution and minimally invasive cellular- and subcellular-level interfaces between recording probes and biological systems, and making such interfaces on a large scale and with high density is of significant importance for mapping activity in the brain and other excitable biological systems.[1a,6] Moreover, the bottom-up paradigm used for the fabrication of nanodevices that we have pioneered[7] enables the preparation of 3D, free-standing, macroporous device arrays that can be utilized as scaffolds for synthetic tissue constructs, and thus, realize monitoring of cellular activity throughout 3D cellular networks.[8] Herein, we discuss the development of novel nanoscale devices for intracellular action potential recording and macroporous nanoelectronic scaffolds for 3D interfacing with synthetic tissue constructs. We focus on field-effect transistor (FET) devices from semiconducting nanowires or nanotubes, in which the active nanowire or nanotube channel serves as the voltage-sensing element. There are several reasons that make this nanoscale FET approach attractive. First, there is no dependence on device/electrolyte interface impedance for an FET voltage sensor,[9] which enables dramatic miniaturization of the recording probes (compared with passive metallic electrodes); this miniaturization of the sensors facilitates both subcellular level resolution and high-density recording. Second, the structure, morphology, physical properties, and corresponding functions of semiconducting nanowires and nanotubes can be well controlled by encoded synthesis, which makes them ideally suited for the hierarchical design of devices.[10]

Novel Nanoscale Devices for Intracellular Action Potential Recording

Kinked Nanowire FET Probes

The main challenge in realizing FET-based intracellular probes is to couple the active channel to the interior of cells in a minimally invasive manner. Unfortunately, the conventional FET geometry, in which the active channel is connected in a linear geometry to large source (S) and drain (D) electrodes, precludes insertion without disruption of cells. Hence, the central question is how to couple a nanoscaled active channel to the intracellular region, while the S/D

electrodes remain extracellular. One efficient way of doing this is to use kinked nanowires, in which the voltage-sensitive active channel—a lightly doped segment—is encoded synthetically at or close to the tip of the kink (Figure 1a and b).[6b,10c] In this structure, the arms of the kink are heavily doped and serve as synthetically defined nanoscale S/D electrodes. A cell probe is then fabricated simply by connecting the nanoscale S/D arms with strained microscale metal interconnects that bend the kinked nanowire up to present the kinked tip to the 3D space (Figure 1c). The heavily doped arms ensure the tip with the nanoFET can access the cell interior and effectively prevent the metal electrodes from disrupting the cell. Because the synthetically defined active part of the kinked nanowire is localized at the tip region, the entire active channel of the FET can be coupled to the interior of the cell; thus ensuring highly sensitive transmembrane potential recording.

To realize cell membrane penetration by the kinked tip, which is required for intracellular action potential recording, we functionalized the kinked nanowire FET devices with phospholipid layers that were similar in structure to the cell membrane.[6b–e,11] When the phospholipid-modified kinked nanowire probes come into contact with a cell, the phospholipid layer can fuse with the cell membrane,[12] which results in spontaneous internalization of the kinked nanowire probe tip into the cell with a tight, high-resistance nanowire/membrane seal. Using phospholipid-modified kinked nanowire probes, we recorded signals from individual cardiomyocyte cells cultured on the PDMS sheets, as shown schematically in Figure 1d.[6b,i] Significantly, we observed a transition from extracellular spikes to intracellular action potential peaks with a concomitant decrease in baseline potential (Figure 1e), following gentle contact of a kinked nanowire probe with a spontaneously firing cardiomyocyte.[6b] This transition occurs without application of an external force, which is consistent with phospholipid-assisted, spontaneous, biomimetic cell membrane penetration. Notably, the stable full-amplitude intercellular action potential peaks recorded after full internalization of the FET nanoprobe (Figure 1f and g) exhibit all of the details of standard cardiac action potentials.[13]

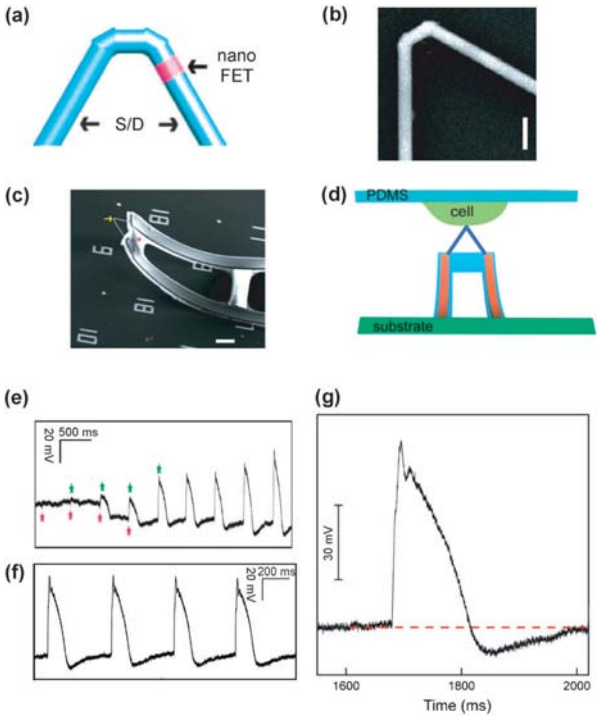

Figure 1. Intracellular action potential recording with kinked nanowire FET devices: a) schematic of a kinked nanowire probe with an encoded active region (pink) obtained by dopant modulation during synthesis. Blue regions are the nanowire source/drain (S/D). b) SEM image of a doubly kinked nanowire with a *cis* configuration. Scale bar, 200 nm; c) A 3D, free-standing, kinked nanowire FET bent probe. The yellow arrow and pink star mark the nanoscale FET and SU-8, respectively. Scale bar, 5 μm. d) Schematic of intracellular recording from cells cultured on polydimethylsiloxane (PDMS) substrate by using kinked nanowire nanoprobes. e) Transition from extra- to intracellular signals during penetration of a kinked nanowire probe into a beating cardiomyocyte. Green and pink stars denote the positions of intra- and extracellular peaks, respectively. f) Steady-state intracellular recording. g) Magnification of an intracellular action potential peak. The red dashed line corresponds to the intracellular rest potential. Reprinted with permission from Ref. [6b].

Xiaojie Duan is an Assistant Professor in the Department of Biomedical Engineering, College of Engineering, at Peking University. She received her Ph.D. in physical chemistry from Peking University in 2007, and pursued postdoctoral studies at Harvard University with Charles Lieber. As a postdoctoral fellow, she developed novel nanoscale devices for action potential recording. Her current research interests include bio-nanomaterials, three-dimensional bio-nano interfaces, large-scale neural activity mapping, and neural tissue engineering and regeneration. She was a recipient of the "National Thousand Talents Plan for Young Scholars" award from the Chinese government.

Charles M. Lieber is the Mark Hyman Professor of Chemistry in the Department of Chemistry and Chemical Biology at Harvard University. He received his Ph.D. from Stanford University (1985) and completed postdoctoral studies at the California Institute of Technology (1987). His research is focused on the chemistry and physics of nanoscale materials with a current emphasis on the synthesis of novel nanowire structures and the design and development of integrated nanoelectronics and nanoelectronic–biological systems. His work has been recognized by numerous awards, including the Wolf Prize in Chemistry (2012) and the Gibbs Medal (2013), and his published papers have been cited more than 67000 times. He is an elected member of the National Academy of Sciences.

Another approach we have implemented for making active kinked nanowire probes involves the incorporation of a p–n junction near the probe tip through synthesis (Figure 2a).[6d] The active channel is localized at the depletion region of the p–n junction,[9c] where the theoretical width of the depletion region could be as small as 10-30 nm;[14] thus allowing potentially very high resolution recording. The tmSGM measurements (Figure 2b) show that the synthetically defined p–n junction region near the kink exhibits a p-type gate response (Figure 2b and c).[6d] The length of the p-depletion region, which defines the spatial resolution of the device, was estimated from the full-width at half-maximum (FWHM) of the SGM line profiles and was found to be 210 nm. This value is lower than the theoretical limit of 10–30 nm[14] and represents an area in which future improvements could be realized.

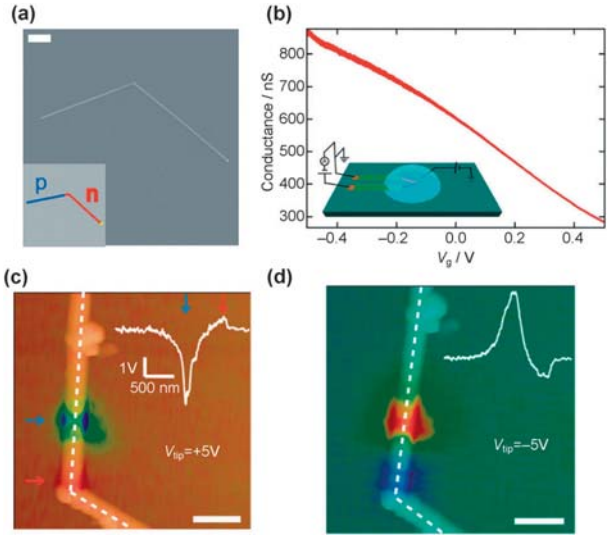

Figure 2. Kinked nanowire p–n junction probes: a) Representative SEM image and schematic (inset) of a kinked p–n junction silicon nanowire with a 120° tip angle. Scale bar, 1 μm. b) Conductance versus water-gate potential recorded from a representative kinked p–n nanowire device in phosphate buffer saline (PBS). Inset: schematic illustration of a conductance versus water-gate experiment setup. c) Superposition of tip-modulated scanning gate microscopy (tmSGM) and AFM topographic images of a representative kinked p–n nanowire device under V_{tip} values of +5 (left) and −5 V (right), respectively. Scale bars, 0.5 μm. The blue/red arrows indicate the p- and n-type depletion/accumulation regions (left panel), respectively; the same positions show accumulation/depletion in the right panel. Insets: line profiles of the tmSGM signal along the white dashed lines about these p- and n-type regions. Reprinted with permission from Ref. [6d].

The strategy of encoding well-defined FET active segments into geometrically controlled nanowire superstructures for 3D, free-standing devices can be extended to prepare a variety of functional bioprobes. For example, we have recently reported three new types of functional kinked nanowires.[15] First, we prepared zero-degree kinked nanowire probes, which had two parallel, heavily doped arms in a U shape and the active nanoscale FET (nanoFET) channel located at the tip of the U (Figure 3a), by encoding three *cis* kinks. Second, we synthesized 60° V-shaped kinked nanowire probes with multiple nanoFETs encoded in series along one arm from the tip (Figure 3b). The multiple nanoFETs open up the possibility of recording from multiple sites with a single probe; a capability truly unique to these bottom-up nanowire structures. Third, we synthesized structures in which two-kink nanowire devices were juxtaposed in a single W shape with nanoFETs integrated at the tip of each of the kinked regions (Figure 3c and d).[15] By encoding multiple nanoFETs in these complex structures and precisely controlling the probe/cell interface, these probes offer high-density multiplexed intracellular recording and/or simultaneous recording of both intra- and extracellular signals (Figure 3e).

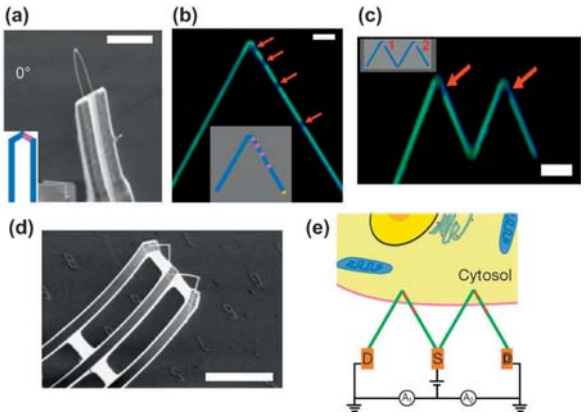

Figure 3. Diverse functional kinked nanowire structures for nanoelectronic bioprobes: a) SEM image of a 3D probe device fabricated by using 30 nm in diameter U-shaped kinked nanowire building blocks. Scale bar, 3 μm. Inset, schematic of a U-shaped kinked nanowire with a tip constructed from three 120° *cis*-linked kinks. The lightly doped n-type nanoFET element (pink) is encoded at the tip and connected by heavily doped n^{++} S/D arms (blue). b) Dark-field optical microscopy image of a KOH-etched kinked nanowire with four nanoFETs. The dark segments correspond to the four lightly doped nanoFET elements (red arrows). Scale bar, 2 μm. Inset, schematic of the probe design. c) Dark-field optical microscopy image of KOH etched W-shaped kinked nanowire. The two dark colored segments correspond to lightly doped nanoFET elements (red arrows) near the two tips. Scale bar, 2 μm. Inset, schematic of the probe design. d) SEM image of a W-shaped, parallel-nanoFET, kinked nanowire probe. Scale bar, 20 μm. e) W-shaped kinked nanowire with multiple nanoFETs (red) illustrated as a bioprobe for simultaneous intra-/extracellular recording. Green indicates heavily doped (n^{++}) S/D nanowire nanoelectrode arms, red highlights the pointlike active nanoFET elements, and gold indicates the fabricated metal interconnects. Reprinted with permission from Ref. [15].

In summary, these kinked nanowire probes demonstrated, for the first time, FET-based intracellular electrical recording of action potentials; they highlighted the potential of FET-based intracellular tools; and, importantly, provided motivation to develop other designs that exhibited unique and complementary characteristics.

Branched Intracellular Nanotube and Active Nanotube FET Probes

To further reduce the size of the FET-based intracellular probes and make the probes more amenable to large-scale, high-density, parallel recording, we developed other designs using nanotube channels to bridge between the inside of the cells and the FET detector elements.[6c,e] The first design, which we termed the branched intracellular nanotube FET (BIT-FET),[6c] involves the use of a vertical or nearly vertical electrically insulating SiO_2 nanotube, which is integrated on top of the FET channel (e.g., a silicon nanowire channel). After the nanotube tip penetrates the cell membrane, the cytosol fills the nanotube and gates the underlying FET; thus enabling the recording of the intracellular transmembrane potential change or action potentials (Figure 4a).[6c] This BIT-FET design uses the tip of controlled-diameter nanotubes to interface to and probe intracellular regime, together with an "impedance-free" FET detector. In this way, it allows for the smallest absolute probe size possible for an electrophysiology tool, and enables interfacing with small subcellular structures, such as neuronal dendrites. In addition, this design is compatible with large-scale, high-density, planar nanoFET arrays,[16] which make parallel recordings from large numbers of probes possible with spatial resolution that would be difficult, if not impossible, to achieve with any other probe.[2]

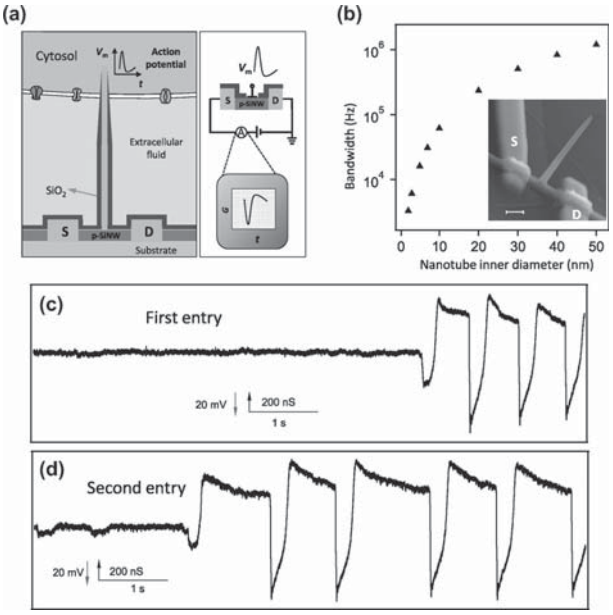

Figure 4. BIT-FET nanoprobes for intracellular action potential recording: a) Schematic illustration of the working principle of the BIT-FET. b) Calculated bandwidth of the BIT-FET device versus the inner diameter of the nanotube for a fixed nanotube length of 1.5 μm. Inset, SEM image of a BIT-FET device. Scale bar, 200 nm. c) Representative trace (conductance versus time) reflecting the transition from extra- to intracellular recording. d) Trace corresponding to the second entry of the BIT-FET nanotube at approximately the same position on the cell as that in c). Reprinted with permission from Ref. [6c].

The BIT-FETs respond selectively and with high sensitivity to the potential change of the solution inside the nanotubes rather than that outside, and thus, meet the requirements for intracellular recording outlined schematically in Figure 4a. In terms of temporal resolution, modeling shows that the BIT-FETs with typical nanotube dimensions (inner diameter, 50 nm; SiO_2 wall thickness, 50 nm; length, 1.5 μm), have a bandwidth in the MHz scale, which is far higher than that necessary for recording even the fastest neuronal action potentials. The bandwidth decreases with decreasing nanotube size, but can still maintain a $\geq$6 kHz value (which is sufficient for recording neuronal action potentials) for nanotube inner diameters as small as 3 nm (Figure 4b).[6c] The small diameters accessible with the BIT-FET suggest that it will be minimally invasive with ultra-high spatial resolution, and thus, be capable of probing the smallest cellular structures, including neuron dendrites and dendritic spines, which are difficult by means of conventional electrophysiology techniques.[6a,17]

We have modified BIT-FET devices with phospholipid layers in a manner similar to that used for the kinked nanowire probes, and used these to investigate spontaneously firing cardiomyocytes.[6c] Notably, BIT-FET devices yield stable intracellular action potentials with standard shapes and full amplitudes from individual beating cardiomyocytes (Figure 4c and d). The ability to record full amplitude action potentials without the need for circuitry to compensate for probe-membrane leakage suggests a tight seal between the nanotube and cell membrane,[1g] which we attribute to the benefits of phospholipid modification; this also demonstrates a clear advantage of the FET-based device versus passive recording techniques. Notably, BIT-FET devices can be retracted from the cell and re-enter at approximately the same position on the same cell to record intracellular action potentials multiple times without affecting the cell (Figure 4d). This capability allows for long-term, stable recording and demonstrates the reliability, robustness, and minimal invasiveness of recording with the BIT-FET devices.[6c]

The nanotube used to couple to the cell interior can also act as the active channel of the FET detector, as shown schematically in Figure 5a.[6e] In this alternative nanotube-based intracellular probe design, the S and D electrodes are fabricated on one end of the nanotube, while leaving the other end free for cell membrane penetration. The cytosol, which fills the nanotube after membrane penetration, can gate the FET from inside the nanotube. Similar to the kinked nanowire probes, strained metal electrodes are used to lift up the nanotube FET and make it accessible to cells (Figure 5b). We term this design an active silicon nanotube transistor (ANTT).[6e] The selective sensitivity to solution inside the nanotube versus that outside enables the faithful recording of intracellular action potentials, as demonstrated from measurements on spontaneously firing cardiomyocytes (Figure 5c). We note that the use of free-standing, microscale, metal electrodes to orient the ANTT probe limits its application in large-scale, high-density recording. This limi-

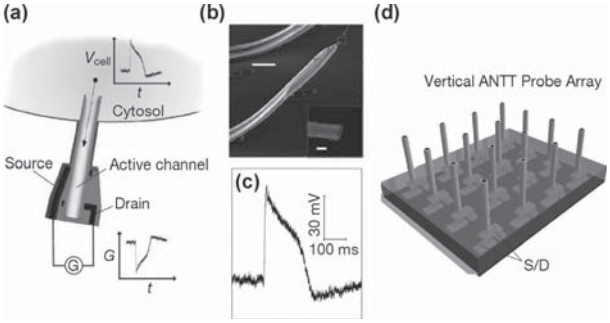

Figure 5. Intracellular recording with the active silicon nanotube transistor (ANTT) probe: a) Schematic illustration of the working principle of the ANTT probe. b) SEM image of an ANTT probe. Scale bar, 10 μm. Inset, close up of the probe tip from the dashed box. Scale bar, 100 nm. c) Representative intracellular action potential peak recorded with an ANTT probe. d) Schematic of chip-based vertical ANTT probe arrays fabricated from epitaxial Ge/Si nanowires for enhanced integration. Reprinted with permission from Ref. [6e].

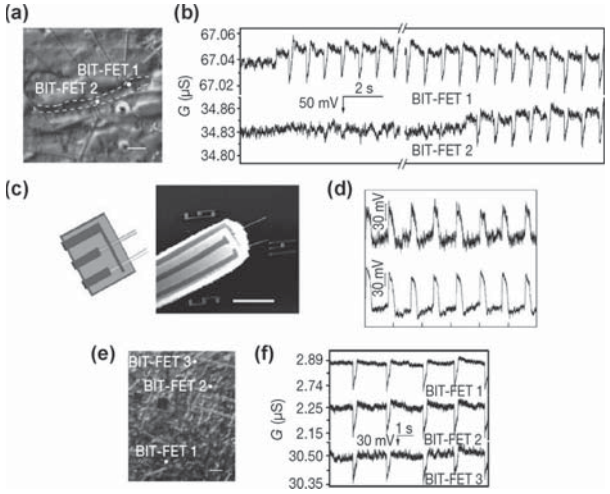

Figure 6. Multiplexed intracellular action potential recording: a) Optical image of two BIT-FET devices (dots) coupled to a single cardiomyocyte cell. The cell boundary is marked by the dashed line. Scale bar, 10 μm. b) Simultaneously recorded traces from the two devices in a), corresponding to the transition from extra- to intracellular recording. c) Design and SEM image of a probe with two independent ANTT devices. Scale bar, 5 μm. d) Intracellular recording from a single cardiomyocyte by using a probe with two independent ANTT devices. The interval between tick marks is 1 s. e) Optical image of three BIT-FET devices coupled to a beating cardiomyocyte cell network. Scale bar, 30 μm. f) Representative intracellular signals recorded simultaneously from the devices shown in e). Reprinted with permission from Ref. [6c,e].

tation could, however, be overcome in the future by preparing vertical nanotube FET arrays (Figure 5d) in a manner similar to work on vertical nanowire FETs.[18]

Simultaneous, Multisite Intracellular Recording

Simultaneous, multisite intracellular recording of action potentials from both single cells and cell networks can be readily achieved by interfacing our novel, independently addressable nanoprobe devices with cells, as shown in Figure 6. The use of phospholipid modification is advantageous for achieving a stable, tight seal between multiple nanoprobes and a cell membrane (or membranes of multiple cells) at the same time. The different probes may penetrate the cell membrane at different times (Figure 6b), but eventually all of them record stable, full-amplitude action potentials; thus demonstrating the possibility of large-scale parallel measurements for neural and cardiac activity mapping.[6c,e]

Nanoscale tools have received considerable attention recently due to their advantages and potential in high spatiotemporal resolution and large-scale brain activity mapping.[1a] Although the nanoprobes reviewed herein have not been prepared on a massive scale, the multiplexed measurements already demonstrate the substantial capabilities of them and the potential for integration on a larger scale. We note that the ability to routinely record full-amplitude action potentials is distinct from recently reported passive metal electrodes, which often yield signals one to two orders of magnitude lower than those expected, even using multiple nanowires/-pillars on a recording electrode.[3b–d] The small size of our FET-based nanoprobes not only makes it possible for unprecedented high-density device arrays, which are critical for cellular and even sub-cellular resolution mapping, but also yields minimal perturbation of the cells and/or tissues under study. Moreover, our studies have shown that phospholipid modification can facilitate cell membrane penetration and yield stable, long-term recording from such nanoprobe arrays. We believe that the nanoprobes discussed herein represent great candidates for use in brain activity mapping and related research,[1a] can extend substantially the scope of fundamental and applied electrophysiology studies, and contribute to areas such as high-throughput drug screening.[1c–e]

Merging Nanoelectronics with Artificial Tissues Seamlessly in 3D

Preparation of 3D Macroporous Nanoelectronic Networks

We recently described, for the first time, how nanoelectronic networks can be seamlessly merged with living tissues in 3D.[8] Conceptually, this merging can be achieved in three basic steps as follows (Figure 7): 1) fabrication of the nanoelectronic network in 2D with underlying sacrificial layers and substrate support (step A, Figure 7); 2) removal of the sacrificial layers to release the nanoelectronic network to yield 3D, free-standing nanoelectronic scaffolds (nanoES), for which the nanoES is used alone or combined with traditional tissue scaffold materials (step B, Figure 7);[19] and 3) cell seeding and culture on the nanoES to yield 3D nanoelectronic–tissue hybrids (step C, Figure 7). In this new paradigm, the critical advance corresponds to the nanoES. The key features of the nanoES that enable seamless 3D merging can be enumerated as follows: 1) a macroporous elec-

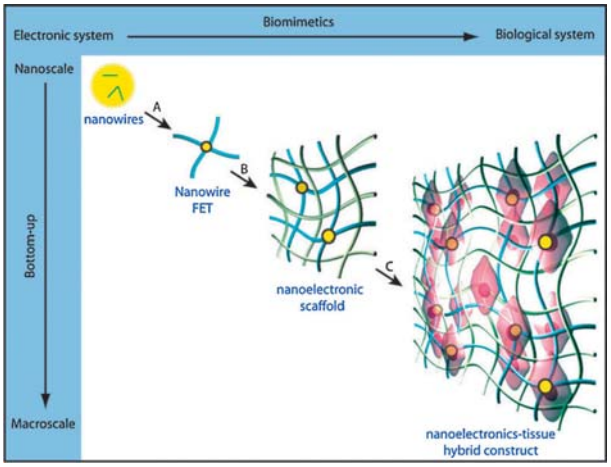

Figure 7. Merging nanoelectronics with artificial tissues seamlessly in three dimensions. Reprinted with permission from Ref. [8a].

tronic network (e.g., >95% porosity) to enable 3D interpenetration of cells in the final hybrid tissue; 2) structural dimensions in the nano- to micrometer size scale to mimic well-studied scaffold materials used for tissue engineering; 3) 3D interconnectivity and addressability of the electronic devices; and 4) mechanical properties similar to those of natural tissue (e.g., much softer than normal electronics).

We met the above constraints with the fabrication of two basic types of nanoES, and exploited these different nanoES for the creation of innervated tissues with neurons, cardiomyocytes, and smooth muscle cells. First, we designed and realized reticular nanoES in which designed stress in the bi- or trimetallic interconnects induced self-bending and self-organization to yield a 3D scaffold with interconnected and addressable nanowire FET sensors (Figure 8a).[8a] Reconstructed 3D confocal fluorescence images of a typical reticular scaffold (Figure 8b) shows clearly the 3D interconnected structure. A magnified SEM image of one of the kinked nanowire FET sensor elements in the nanoES is shown in Figure 8c.

The second basic class of nanoES, the mesh nanoES, is based on a 2D macroporous nanoelectronic network sheets (Figure 9a).[8] A regular nanoelectronic devices array with a structural backbone is patterned by a combining nanowire assembly and conventional 2D lithography on the 2D supporting substrate (Figure 9b). After removal of the underlying sacrificial layer, the free-standing and flexible 2D macroporous nanoelectronic network sheets can be organized into 3D macroporous structures by either directed assembly from manual manipulation, such as rolling (Figure 9c), or stress-induced self-assembly (Figure 9d). During the fabrication of these nanoES, functional nanoelectronic elements, such as nanowires with variations in composition, morphology, and doping, can be incorporated for diverse functionality, including devices for sensors,[9b,20a] light-emitting diodes,[20b] logic and memory,[16,20c] and energy production and storage (Figure 9e).[20d–f]

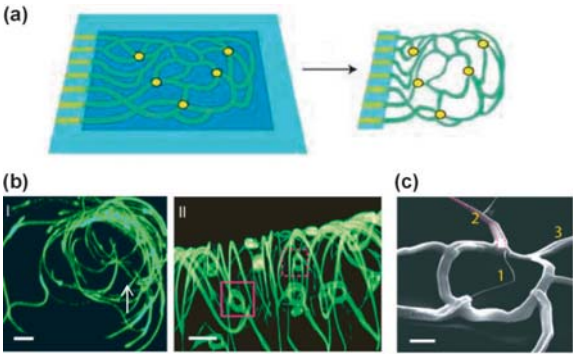

Figure 8. Reticular nanoES: a) Device fabrication schematics for reticular nanoES. Light blue: silicon oxide substrates; blue: nickel sacrificial layers; green: nanoES; yellow dots: individual nanowire FETs. b) 3D reconstructed confocal fluorescence micrographs of reticular nanoES viewed along the y (I) and x (II) axes. Solid and dashed open magenta squares indicate two nanowire FET devices located on different planes along the x axis. Scale bars, 20 μm. c) SEM image of a single kinked nanowire FET within a reticular scaffold, showing 1) the kinked nanowire, 2) metallic interconnects (dashed magenta lines), and 3) the SU-8 backbone. Scale bar, 2 μm. Reprinted with permission from Ref. [8a].

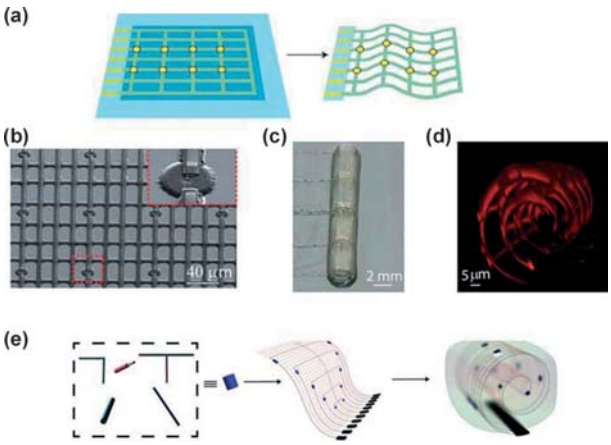

Figure 9. Mesh nanoES: a) Device fabrication schematics for mesh nanoES. The color designation is same as that used in Figure 8a. b) SEM image of a 2D macroporous nanoelectronic network before release from the substrate. Inset: magnification of the region enclosed by the small red dashed box containing a single nanowire device. c) Photograph of a manually scrolled up 3D macroporous nanoelectronic network. d) 3D reconstructed confocal fluorescence image of the self-organized 3D macroporous nanoelectronic network viewed along the x axis. e) Strategy for preparing 3D macroporous nanoelectronic networks by using nanowires with variations in composition, morphology, and doping for diverse device functionality. Reprinted with permission from Ref. [8].

In the above nanoES, the 3D networks can have porosities larger than 99%, contain hundreds of addressable nanowire devices and have feature sizes from the 1–10 μm scale (for electrical and structural interconnections) to the 10 nm scale (for device elements). Importantly, typical 3D macroporous nanoelectronic networks have very low effective bending stiffness values from 0.0038 to 0.0378 $nN\,m^{-1}$.[8b] These values, which can be readily tuned by design and fab-

rication over a much wider range, are comparable with synthetic and natural extracellular matrices (ECMs);[19] thus making them an ideal scaffold for innervating synthetic neural and cardiac tissue.

Three-Dimensional Nanoelectronics/Tissue Hybrids

After hybridization with a conventional scaffold, such as Matrigel, poly(lactic-*co*-glycolic acid) (PLGA), the nanoES have been used for 3D culture of neurons, cardiomyocytes, and smooth muscle cells.[8] Reconstructed 3D confocal micrographs from a two-week culture of rat hippocampal neurons on the reticular nanoES/Matrigel (Figure 10a and b) show clearly neurons with a high density of spatially interconnected neurites that penetrate seamlessly into the reticular nanoES (Figure 10a), sometimes passing through the ring structures supporting individual nanowire FET sensors (Figure 10b). Three-dimensional cardiac tissue was also achieved from a hybrid nanoES/PLGA scaffold following seeding and culture of cardiomyocytes. Confocal fluorescence microscopy of a typical cardiac 3D culture (Figure 10c) revealed a high density of cardiomyocytes in close contact with the nanoES components. Epifluorescence micrographs of cardiac cells on the surface (Figure 10d) further show striations characteristic of cardiac tissue.[19a,c]

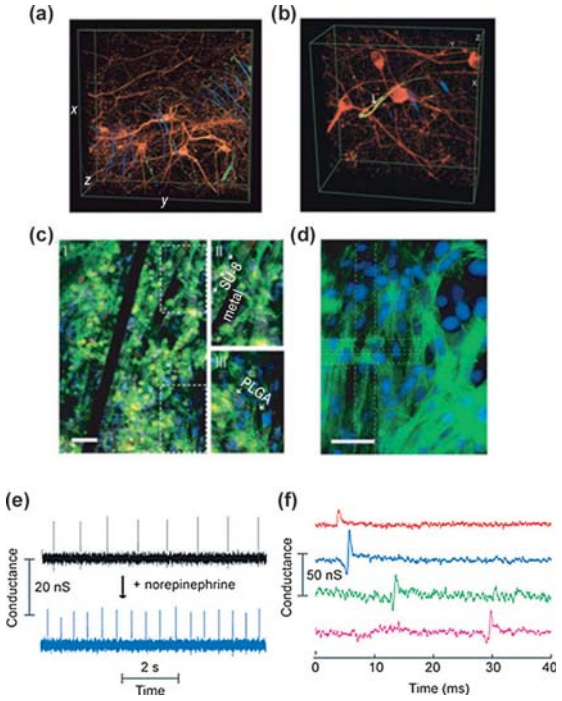

Figure 10. 3D nanoelectronics/tissue hybrids: a) and b) 3D reconstructed confocal images of rat hippocampal neurons after a two-week culture on a reticular nanoES. The white arrow highlights a neurite passing through a ring-like structure supporting a nanowire FET. Dimensions in a: $x=317\,\mu m$, $y=317\,\mu m$, $z=100\,\mu m$; in b: $x=127\,\mu m$, $y=127\,\mu m$, $z=68\,\mu m$. c) Confocal fluorescence micrographs of a synthetic cardiac patch. (II and III); close-up views of the upper (II) and lower (III) dashed regions in I are also shown. Scale bar, 40 μm. d) Epifluorescence micrograph of the surface of the cardiac patch. Green: α-actin; blue: cell nuclei. The dashed lines outline the position of the S/D electrodes. Scale bar, 40 μm. e) Conductance versus time traces recorded from a single nanowire FET before (black) and after (blue) applying noradrenaline. f) Multiplexed electrical recording of extracellular field potentials from four nanowire FETs at different depths in a nanoES/cardiac hybrid. Reprinted with permission from Ref. [8a].

Significantly, cytotoxicity tests showed minimal difference in cell viability for culture in the scaffold with and without nanoES.[21] Furthermore, the original nanowire FET device characteristics were retained after 3D organization of the nanoES, scaffold hybridization, and cell culture up to at least 12 weeks.[8] The capability of the nanoES for long-term culture and monitoring enables a number of in vitro studies, including drug screening assays with these synthetic neural and cardiac tissues, and suggests possibilities for implants and new types of chronic recording probes.

The 3D sensory capabilities of the nanoES were demonstrated by recording of extracellular action potentials by using nanowire FET devices within a nanoES/cardiac tissue hybrid, as shown in Figure 10e, in which a nanowire FET about 200 μm below the construct surface gives standard signals with a high SNR and responds to the stimulatory drug noradrenaline with a clear increase in action potential firing frequency. In addition, multiplexed recording from a coherently beating nanoES/cardiac construct demonstrated submillisecond temporal resolution from the four nanowire FETs with separations up to 6.8 mm within the 3D innervated tissue sample (Figure 10f).[8a]

Vascular constructs (Figure 11a) with embedded nanoelectronics in 3D space were also achieved by culturing human aortic smooth muscle cells (HASMCs) on 2D mesh nanoES, and then rolling the hybrid nanoES/HASMC sheets (Figure 11b) into multilayer 3D tubular structures, as shown in Figure 11c.[8a] When a solution with constant pH flowed through the inner (lumen) region of the vascular construct and the pH of the extravascular solution changed stepwise (Figure 11d), the nanowire FETs in the outermost layer showed a stepwise decrease in conductance with a sensitivity of about 32 mV per pH unit, while only minor baseline fluctuations were observed for the nanowire FETs in the innermost layer (closest to the lumen). This result demonstrates the potential ability of the embedded nanowire FETs to detect inflammation, ischemia, tumor microenvironments, or other forms of metabolic acidosis[22] in the implanted devices, which is important to many aspects of biomedical research and healthcare.

Multifunctional 3D Macroporous Nanoelectronic Networks

Multifunctionality can be incorporated into the 3D nanoelectronic macroporous network by assembly of nanowire building blocks to yield devices such as photodetectors, light-emitting diodes, and strain sensors. The conductivity of nanowire FETs change upon illumination (Figure 12a), which allows the nanoFET to function as a photodetector. Hence, during optical imaging of nanoelectronics/tissue hybrids, this photo-sensitivity can be utilized to determine the

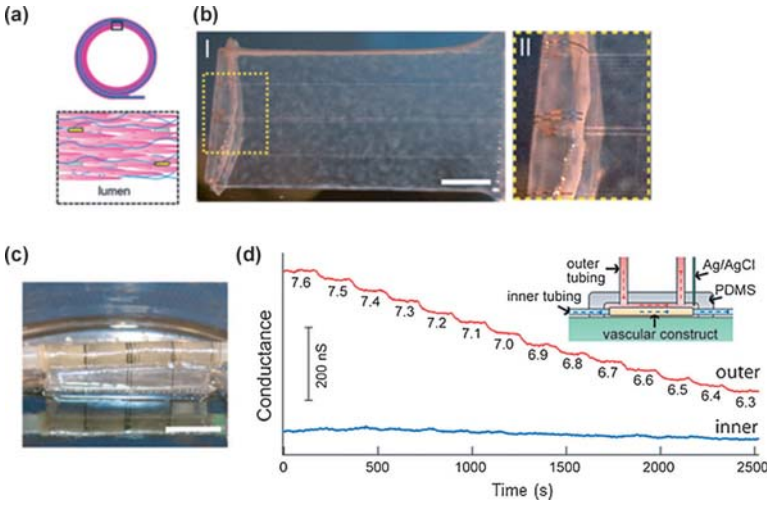

Figure 11. Synthetic vascular construct for 3D sensing: a) Schematic of the smooth muscle nanoES. The upper panels are the side view, and the lower one is a close-up view. Grey: mesh nanoES; blue fibers: collagenous matrix secreted by HASMCs; yellow dots: nanowire FETs; pink: HASMCs. b) I) Photograph of a single HASMC sheet cultured with sodium L-ascorbate on a nanoES. II) Magnification of the dashed area in I). Scale bar, 5 mm. c) Photograph of the vascular construct after rolling into a tube and maturation in a culture chamber for three weeks. Scale bar, 5 mm. d) Changes in conductance over time for nanowire FET devices located in the outer- (red) and innermost (blue) layers. The inset shows a schematic of the experimental setup. The outer tubing delivered bathing solutions with varying pH (red dashed lines and arrows); the inner tubing delivered solutions with fixed pH (blue dashed lines and arrows). Reprinted with permission from Ref. [8a].

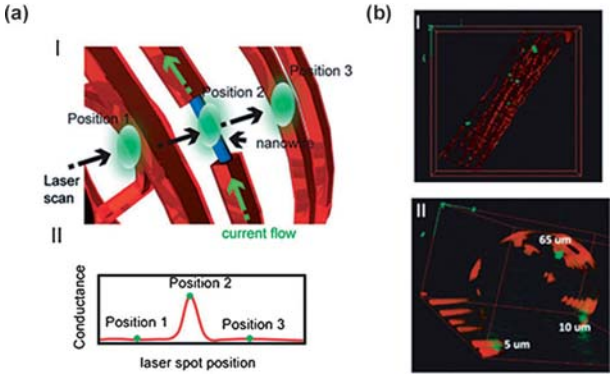

Figure 12. 3D macroporous nanoelectronic photodetectors and device localization: a) Schematics of the nanowire photodetector characterization. Green ellipse, scanned laser spot; blue cylinder, nanowire; orange, SU-8 mesh network (I). Changes in the conductance of the nanowire during scanning (II) can be correlated with position. Green spots in II) represent the laser spots in I). b) 3D reconstructed photocurrent image overlapped with confocal microscopy imaging shows the spatial correlation between nanowire photodetectors and the SU-8 framework in 3D. Green, false color of the photocurrent signal; orange (rhodamine 6G), SU-8 mesh network. Dimensions in I: $x=317$ μm, $y=317$ μm, $z=53$ μm; II: $x=127$ μm, $y=127$ μm, $z=65$ μm. The white numbers in II) indicate the heights of the nanowire photodetectors. Reprinted with permission from Ref. [8b].

positions of the nanowire FETs throughout the 3D space of the constructs at high resolution (Figure 12b).[8b]

In addition, the large piezoresistance[23] of silicon nanowires allows them to function as strain sensors.[24] Our measurements show that the nanowire FETs can have a conductance change of 20 nS for 1% tensile strain.[8b] By calibrating the strain sensitivity for each nanowire FET, the embedded nanowire FET array can be used to map the strain distributions inside 3D macroporous nanoelectronic network/elastomer or tissue hybrid materials (Figure 13).[8b] Furthermore, the 1D geometry of nanowires gives these strain sensors nearly perfect directional selectivity, and thus, by controlling the orientation of the nanowire devices to be parallel and perpendicular to the cylinder axis, mapping of the three components of the strain field is possible.

The concept and strategy for making 3D macroporous nanoelectronic networks can be further extended to other materials and device designs to enable greater functionality, not only

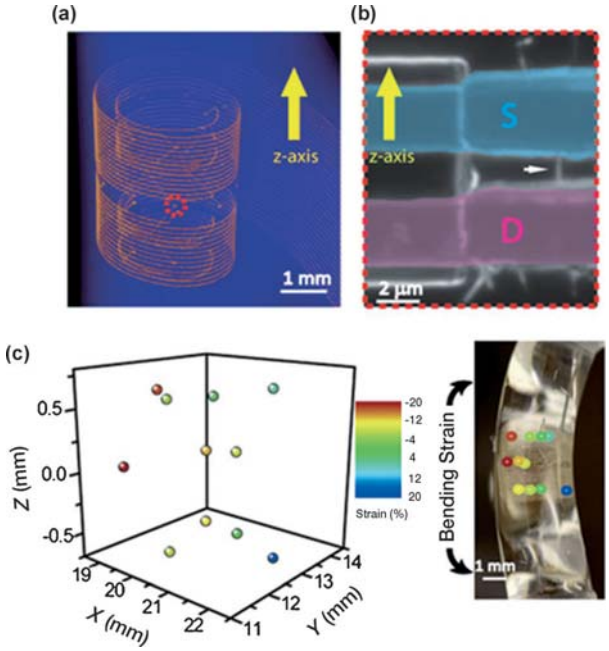

Figure 13. The 3D macroporous nanoelectronic strain sensors and strain field mapping: a) Micro-CT 3D reconstruction of the mesh network embedded in a piece of elastomer. b) Dark-field microscopy image of a typical nanowire device indicated by a red dashed circle in a). The white arrow points to a nanowire. c) and d) The 3D mapping of the strain field applied in the deformed elastomer recorded with the nanowire strain sensors. The detected strains are marked at the device positions in the cylinder image. Reprinted with permission from Ref. [8b].

for the detection of various cellular activities and physiochemical information, but also for feedback (e.g., electrical stimulation or drug release) throughout the 3D space of the tissue constructs. We believe that the further development and application of these 3D macroporous nanoelectronics network will make a profound impact on many research areas, for example, 1) brain activity mapping, for which the new 3D recording capability is expected to allow recording of large-scale deep tissue or brain activity that is difficult with other methods;[1a,2,6a] 2) in vitro pharmacological studies, for which 3D tissue models will provide a more robust link to in vivo disease treatment than 2D cell cultures;[25] and 3) tissue engineering studies, for which 3D sensory and intervention abilities will maintain fine control on synthetic tissue growth and function.[4a,26]

Summary and Outlook

To date, a diverse toolbox of transistor-based nanoprobes has been developed for action potential recording. These new FET nanoprobes have a number of unique features, including minimal invasiveness, high spatiotemporal resolution, and the capability to be scaled for large-number, high-density recording. Furthermore, these nanoprobes can be integrated in 3D by making macroporous nanoelectronics networks (nanoES) to implement recording and sensory capabilities throughout 3D space in tissues and/or artificial tissue constructs. All of these results represent substantial advances in nanoelectronics/biology interfacing, and we believe will serve as the foundation for new fundamental studies[1a,6h,27] and novel directions in biomedical research and applications,[28] including brain activity mapping, tissue engineering, stem cell studies, neural implantation, and prostheses (Figure 14).

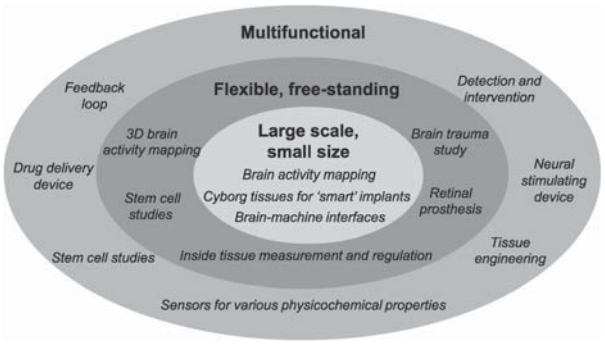

Figure 14. Overview of the new fundamental studies and novel directions in biomedical research and applications enabled by progress at the nanoelectronics/biology interface. These new studies benefit from the unique features of nanoelectronics.

Acknowledgements

This work was supported by the NIH Director's Pioneer Award (5DP1OD003900), the McKnight Foundation Technological Innovations in Neurosciences Award, the National Security Science and Engineering Faculty Fellow (NSSEFF) award (N00244-09-1-0078), a "National Thousand Talents Plan" award from China, and the National Basic Research Program of China (No. 2014CB932500). We also acknowledge Prof. Chunli Bai for his seminal contributions to nanoscience in China, including the introduction of scanning probe microscopy at the beginning of the field, and for his visionary leadership in China, defining critical research directions in nanoscience as well as science and technology policy as a whole as Vice President and President of the Chinese Academy of Science (CAS).

[1] a) C. Koch, R. C. Reid, *Nature* **2012**, *483*, 397–398; b) B. Hille, *Ion Channels of Excitable Membranes*, *3rd ed.*, Sinauer Associates Inc., Sunderland, **2001**; c) J. Dunlop, M. Bowlby, R. Peri, D. Vasilyev, R. Arias, *Nat. Rev. Drug Discovery* **2008**, *7*, 358–368; d) T. Meyer, K. H. Boven, E. Gunther, M. Fejtl, *Drug Saf.* **2004**, *27*, 763–772; e) S. Dhein, F. W. Mohr, M. Delmar, *Practical Methods in Cardiovascular Research*, Springer, Berlin, **2005**, pp. 215–453; f) R. M. Wightman, *Science* **2006**, *311*, 1570–1574; g) W. L. C. Rutten, *Annu. Rev. Biomed. Eng.* **2002**, *4*, 407–452.

[2] a) A. Molleman, *Patch Clamping: An Introductory Guide to Patch Clamp Electrophysiology*, Wiley, Chichester, **2003**; b) R. D. Purves, *Microelectrode Methods for Intracellular Recording and Ionophoresis*, Academic Press, Burlington, **1981**.

[3] a) J. Erickson, A. Tooker, Y.-C. Tai, J. Pine, *J. Neurosci. Methods* **2008**, *175*, 1–16; b) A. Hai, J. Shappir, M. E. Spira, *Nat. Methods* **2010**, *7*, 200–202; c) C. Xie, Z. Lin, L. Hanson, Y. Cui, B. Cui, *Nat. Nanotechnol.* **2012**, *7*, 185–190; d) J. T. Robinson, M. Jorgolli, A. K. Shalek, M.-H. Yoon, R. S. Gertner, H. Park, *Nat. Nanotechnol.* **2012**, *7*, 180–184.

[4] T. Dvir, B. P. Timko, D. S. Kohane, R. Langer, *Nat. Nanotechnol.* **2011**, *6*, 13–22.

[5] a) B. P. Timko, T. Cohen-Karni, G. Yu, Q. Qing, B. Tian, C. M. Lieber, *Nano Lett.* **2009**, *9*, 914–918; b) J. Viventi, D.-H. Kim, L. Vigeland, E. S. Frechette, J. A. Blanco, Y.-S. Kim, A. E. Avrin, V. R Tiruvadi, S.-W. Hwang, A. C Vanleer, D. F Wulsin, K. Davis, C. E Gelber, L. Palmer, J. Van der Spiegel, J. Wu, J. Xiao, Y. Huang, D. Contreras, J. A Rogers, B. Litt *Nat. Neurosci.* **2011**, *14*, 1599–1605; c) D.-H. Kim, N. Lu, R. Ma, Y.-S. Kim, R.-H. Kim, S. Wang, J. Wu, S. M. Won, H. Tao, A. Islam, K. J. Yu, T.-i. Kim, R. Chowdhury, M. Ying, L. Xu, M. Li, H.-J. Chung, H. Keum, M. McCormick, P. Liu, Y.-W. Zhang, F. G. Omenetto, Y. Huang, T. Coleman, J. A. Rogers, *Science* **2011**, *333*, 838–843.

[6] a) M. Scanziani, M. Hausser, *Nature* **2009**, *461*, 930–939; b) B. Tian, T. Cohen-Karni, Q. Qing, X. Duan, P. Xie, C. M. Lieber, *Science* **2010**, *329*, 830–834; c) X. Duan, R. Gao, P. Xie, T. Cohen-Karni, Q. Qing, H. S. Choe, B. Tian, X. Jiang, C. M. Lieber, *Nat. Nanotechnol.* **2012**, *7*, 174–179; d) Z. Jiang, Q. Qing, P. Xie, R. Gao, C. M. Lieber, *Nano Lett.* **2012**, *12*, 1711–1716; e) R. Gao, S. Strehle, B. Tian, T. Cohen-Karni, P. Xie, X. Duan, Q. Quan, C. M. Lieber, *Nano Lett.* **2012**, *12*, 3329–3333; f) F. Patolsky, B. P. Timko, G. Yu, Y. Fang, A. B. Greytak, G. Zheng, C. M. Lieber, *Science* **2006**, *313*, 1100–1104; g) T. Cohen-Karni, Q. Qing, Q. Li, Y. Fang, C. M. Lieber, *Nano Lett.* **2010**, *10*, 1098–1102; h) B. P. Timko, T. Cohen-Karni, Q. Qing, B. Tian, C. M. Lieber, *IEEE Trans. Nanotechnol.* **2010**, *9*, 269–280; i) T. Cohen-Karni, B. P. Timko, L. E. Weiss, C. M. Lieber, *Proc. Natl. Acad. Sci. USA* **2009**, *106*, 7309–7313; j) T. Cohen-Karni, D. Casanova, J. Cahoon, Q. Qing, D. Bell, C. M. Lieber, *Nano Lett.* **2012**, *12*, 2639–2644; k) Q. Qing, S. K. Pal, B. Tian, X. Duan, B. P. Timko, T. Cohen-Karni, V. N. Murthy, C. M. Lieber, *Proc. Natl. Acad. Sci. USA* **2010**, *107*, 1882–1887.

[7] W. Lu, C. M. Lieber, *Nat. Mater.* **2007**, *6*, 841–850.

[8] a) B. Tian, J. Liu, T. Dvir, L. Jin, J. H. Tsui, Q. Qing, Z. Suo, R. Langer, D. S. Kohane, C. M. Lieber, *Nat. Mater.* **2012**, *11*, 986–994;

b) J. Liu, C. Xie, X. Dai, L. Jin, W. Zhou, C. M. Lieber, *Proc. Natl. Acad. Sci. USA* **2013**, *110*, 6694–6699.
[9] a) O. J. Prohaska, F. Olcaytug, P. Pfundner, H. Dragaun, *IEEE Trans. Biomed. Eng.* **1986**, *33*, 223–229; b) F. Patolsky, G. Zheng, C. M. Lieber, *Anal. Chem.* **2006**, *78*, 4260–4269; c) S. M. Sze, K. K. Ng, *Physics of Semiconductor Devices*, *3rd ed.*, Wiley Interscience, **2006**.
[10] a) X. Jiang, B. Tian, J. Xiang, F. Qian, G. Zheng, H. Wang, L. Mai, C. M. Lieber, *Proc. Natl. Acad. Sci. USA* **2011**, *108*, 12212–12216; b) C. Yang, Z. Zhong, C. M. Lieber, *Science* **2005**, *310*, 1304–1307; c) B. Tian, P. Xie, T. J. Kempa, D. C. Bell, C. M. Lieber, *Nat. Nanotechnol.* **2009**, *4*, 824–829; d) Z. Pan, Z. Dai, Z. Wang, *Science* **2001**, *291*, 1947–1949; e) X. Wang, C. J. Summers, Z. Wang, *Nano Lett.* **2004**, *4*, 423–426.
[11] C. A. Keller, K. Glasmästar, V. P. Zhdanov, B. Kasemo, *Phys. Rev. Lett.* **2000**, *84*, 5443–5446.
[12] a) B. D. Almquist, N. A. Melosh, *Proc. Natl. Acad. Sci. USA* **2010**, *107*, 5815–5820; b) L. V. Chernomordik, M. M. Kozlov, *Nat. Struct. Mol. Biol.* **2008**, *15*, 675–683.
[13] D. M. Bers, *Nature* **2002**, *415*, 198–205.
[14] L. Weber, E. Gmelin, *Appl. Phys. A* **1991**, *53*, 136–140.
[15] L. Xu, Z. Jiang, Q. Qing, L. Mai, Q. Zhang, C. M. Lieber, *Nano Lett.* **2013**, *13*, 746–751.
[16] H. Yan, H. S. Choe, S. W. Nam, Y. Hu, S. Das, J. F. Klemic, J. C. Ellenbogen, C. M. Lieber, *Nature* **2011**, *470*, 240–244.
[17] J. T. Davie, M. H. P. Kole, J. J. Letzkus, E. A. Rancz, N. Spruston, G. J. Stuart, M. Hausser, *Nat. Protoc.* **2006**, *1*, 1235–1247.
[18] a) J. Goldberger, A. I. Hochbaum, R. Fan, P. Yang, *Nano Lett.* **2006**, *6*, 973–977; b) T. Bryllert, L. Wemersson, L. E. Froberg, L. Samuelson, *IEEE Electron Device Lett.* **2006**, *27*, 323–325.
[19] a) E. S. Place, J. H. George, C. K. Williams, M. M. Stevens, *Chem. Soc. Rev.* **2009**, *38*, 1139–1151; b) G. C. Engelmayr, Jr., M. Cheng, C. J. Bettinger, J. T. Borenstein, R. Langer, L. E. Freed, *Nat. Mater.* **2008**, *7*, 1003–1010; c) Y. Sapir, O. Kryukov, S. Cohen, *Biomaterials* **2011**, *32*, 1838–1847; d) P. J. Hanley, A. A. Young, I. J. LeGrice, S. G. Edgar, D. S. Loiselle, *J. Physiol.* **1999**, *517*, 831–837.
[20] a) Y. Cui, Q. Wei, H. Park, C. M. Lieber, *Science* **2001**, *293*, 1289–1292; b) F. Qian, S. Gradecak, Y. Li, C. Y. Wen, C. M. Lieber, *Nano Lett.* **2005**, *5*, 2287–2291; c) J. Xiang, W. Lu, Y. Hu, Y. Wu, H. Yan, C. M. Lieber, *Nature* **2006**, *441*, 489–493; d) Y. Qin, X. D. Wang, Z. L. Wang, *Nature* **2008**, *451*, 809–813; e) C. K. Chan, H. Peng, G. Liu, K. McIlwrath, X. Zhang, R. A. Huggins, Y. Cui, *Nat. Nanotechnol.* **2008**, *3*, 31–35; f) B. Tian, X. Zheng, T. J. Kempa, Y. Fang, N. Yu, G. Yu, J. Huang, C. M. Lieber, *Nature* **2007**, *449*, 885–890.
[21] T. Xu, P. Molnar, G. Cassie, M. Das, T. Boland, J. J. Hickman, *Biomaterials* **2009**, *30*, 4377–4383.
[22] a) D. Neri, C. T. Supuran, *Nat. Rev. Drug Discovery* **2011**, *10*, 767–777; b) J. A. Kraut, N. E. Madias, *Nat. Rev. Nephrol.* **2010**, *6*, 274–285.
[23] R. He, P. Yang, *Nat. Nanotechnol.* **2006**, *1*, 42–46.
[24] C. H. Lee, D. R. Kim, X. Zheng, *Proc. Natl. Acad. Sci. USA* **2010**, *107*, 9950–9955.
[25] a) D. Huh, B. D. Matthews, A. Mammoto, M. Montoya-Zavala, H. Y. Hsin, D. D. Ingber, *Science* **2010**, *328*, 1662–1668; b) M. Baker, *Nature* **2011**, *471*, 661–665.
[26] a) T. Dvir, B. P. Timko, M. D. Brigham, S. R. Naik, S. S. Karajanaqi, O. Levy, H. Jin, K. K. Parker, R. Langer, D. S. Kohane, *Nat. Nanotechnol.* **2011**, *6*, 720–725; b) K. Takei, T. Takahashi, J. C. Ho, H. Ko, A. G. Gillies, P. W. Leu, R. S. Fearing, A. Javey, *Nat. Mater.* **2010**, *9*, 821–826.
[27] a) R. K. Wong, D. A. Prince, A. I. Basbaum, *Proc. Natl. Acad. Sci. USA* **1979**, *76*, 986–990; b) F. Guilak, D. M. Cohen, B. T. Estes, J. M. Gimble, W. Liedtke, C. S. Chen, *Cell Stem Cell* **2009**, *5*, 17–26; c) M. P. Lutolf, P. M. Gilbert, H. M. Blau, *Nature* **2009**, *462*, 433–441; d) T. C. Pappas, W. M. S. Wickramanyake, E. Jan, M. Motamedi, M. Brodwick, N. A. Kotov, *Nano Lett.* **2007**, *7*, 513–519.
[28] a) S. F. Gizler, *Neurotherapeutics* **2008**, *5*, 147–162; b) A. Caspi, J. D. Dorn, K. H. McClure, M. S. Humayun, R. J. Greenberg, M. J. McMahon, *Arch. Ophthalmol.* **2009**, *127*, 398–401; c) Z. Yu, O. Graudejus, C. Tsay, S. P. Lacour, S. Wagner, B. Morrison III., *J. Neurotrauma* **2009**, *26*, 1135–1145; d) D. H. Szarowski, M. D. Andersen, S. Retterer, A. J. Spence, M. Isaacson, H. G. Craighead, J. N. Turner, W. Shain, *Brain Res.* **2003**, *983*, 23–25; e) R. Biran, D. C. Martin, P. A. Tresco, *Exp. Neurol.* **2005**, *195*, 115–126.

Received: May 4, 2013
Published online: August 15, 2013

